Ceramics International 45 (2019) 10646–10653

Contents lists available at ScienceDirect

Ceramics International

journal homepage: www.elsevier.com/locate/ceramint

Aqueous slip casting of translucent magnesium aluminate spinel: Effects of dispersant concentration and solid loading

Ali Talimian[a,*], Dusan Galusek[a,b]

[a] Department VILA, Centre for Functional and Surface Functionalised Glass (FunGlass), Alexander Dubcek University of Trencin, Trencin, Slovakia
[b] Department VILA – Joint Glass Centre of the IIC SAS, TnUAD, FChPT STU, Študentská 2, 911 50 Trenčín, Slovakia

ARTICLE INFO

Keywords:
Magnesium aluminate spinel
Slip casting
Sintering
Grain growth

ABSTRACT

In the present study, influences of the dispersant concentration and solid loading on the rheological properties of magnesium aluminate spinel suspensions are investigated. Aqueous suspensions of commercial spinel powder were prepared by using a polyelectrolyte dispersing agent up to 5 wt%. The viscosity of suspensions decreases continuously with the increase of dispersant concentration; this enables producing $MgAl_2O_4$ suspensions containing 30 vol% solid-loading (60 wt%). Green bodies with a relative density larger than 50% were produced from the suspensions; translucent spinel was obtained after sintering at 1550 °C for 2 h.

1. Introduction

Magnesium aluminate spinel is a material with excellent mechanical performance, chemical durability and thermal stability [1–5]. Spinel also has attracted a lot of attention due to its optical properties [3,6,7]. Having cubic structure, transparent polycrystalline spinel bodies can be obtained via producing a highly dense body by removing pores and scattering centres. However, eliminating the porosity is a difficult task in practice, due to the low sintering rate of spinel [8–11]. A dense body is usually produced through pre-sintering followed by hot isostatic pressing [12–14]. Although high-temperature sintering results in high-density ceramics, the extension of sintering time and prolonged sintering regimes usually fail to remove large pores originating from the shaping process. Moreover, pore coalescence can also occur resulting in the production of larger pores [15,16]. Therefore, obtaining a homogeneous green body is the very prerequisite for fabricating transparent spinel [17].

While the densification of transparent polycrystalline spinel has been discussed extensively in literature, less attention has been paid to the fabrication of a homogeneous green structure which densifies straightforwardly [10,13,18]. Highly homogenous compacts can be obtained through colloidal processes such as slip casting; particles can be rearranged easily in a well-dispersed suspension producing highly packed green bodies [7,19,20].

There are limited works on the fabrication of transparent spinel shaped by slip casting: in some cases, electrostatic mechanisms were utilised to prepare aqueous suspensions of spinel powder [21–23]; in other studies, the suspensions were produced by exclusively using dispersing agents [1,17,23–27]. The pH modification introduces an extra step in suspension preparation; moreover, some chemicals can introduce alkali ions promoting abnormal grain growth during sintering and impairing the performance of sintered bodies such as mechanical properties and thermal shock resistance [11,28]. Also, the solid loading of spinel in suspensions is limited: green bodies are produced using a certain solid fraction, usually lower than 20 vol%. This requires the green pellets to be compacted further by cold isostatic pressing [17,19,24,25]. The knowledge on the rheological behaviour of high solid fraction suspensions is limited.

In the present work, suspensions of a commercial spinel powder are prepared by exclusively using alkali-free dispersing agent; impacts of the dispersant concentration and solid fraction on the rheological behaviour of $MgAl_2O_4$ are investigated, and the maximum concentration of solid particles is determined. Furthermore, the sintering behaviour of green compacts prepared by slip casting and fabrication of highly dense bodies are discussed.

2. Experimental procedure

A commercial $MgAl_2O_4$ spinel powder (Biakolax S30CR, Baikowski, Paris, France) was used in this study. The powder has a BET specific surface area of 26 $m^2 g^{-1}$ with a median particle size (d_{50}) of 0.2 μm according to the data provided by the supplier.

Aqueous suspensions with a solid loading of $MgAl_2O_4$ between 3 and 30 vol% were prepared by ball milling a mixture of the powder, de-

* Corresponding author.
E-mail address: ali.talimian@tnuni.sk (A. Talimian).

https://doi.org/10.1016/j.ceramint.2019.02.134
Received 8 November 2018; Received in revised form 31 January 2019; Accepted 19 February 2019
Available online 20 February 2019

ionised water and Dolapix CE 64 dispersant (Zschimmer & Schwarz, Lahnstein, Germany) in Polypropylene bottles using zirconia milling balls, (YTZ®,Tosoh, Tokyo, Japan) for 8–72 h. The dispersant concentration was varying between 0.05 and 8 wt% of the solid powder in the suspensions.

After ball milling for 24 h, the suspensions were de-aired and slip-cast in cylindrical moulds comprising a silicon rubber wall and a porous gypsum bottom. The produced bodies were dried at room temperature overnight and, afterwards, the remaining moisture was removed by drying at 80 °C for 48 h in a convection dryer. The dispersing agent was burnt out at 450 °C for 30 min, and the samples were sintered at 1550 °C for 120 min in an electric furnace under ambient conditions using the heating rate of 10 °C min^{-1}. Part of the samples prepared from concentrated slurries containing 30 vol% solid fraction of $MgAl_2O_4$, was removed from the furnace at various temperatures between 1450 and 1550 °C after isothermal heating ranging from 0 to 240 min. These samples were used to evaluate the densification as well as the change of residual porosity during sintering.

Dynamic light scattering (DLS) was employed to determine the particle size distribution in suspensions using a particle size analyser (NanoBrook 90Plus, Brookhaven, NY, USA); the measured suspensions were diluted to ~100 ppm by the addition of suspensions to de-ionised water and mixing in an ultrasonic bath for five minutes. The shear stress and viscosity of slurries were measured as a function of applied shear rate in the range 1–450 s^{-1}, at the constant temperature of 20 °C using a controlled stress rheometer (Haake MARS III, Thermo-Scientific, Berlin, Germany). In order to obtain samples with similar thermo-rheological history, all slurries were subjected to a shear rate of 450 s^{-1} for 60 s followed by a rest for 30 s.

The density of sintered bodies was evaluated using Archimedes' principle.

The burn-out point of residual dispersant in green bodies were determined using a Simultaneous Thermal Analyser (STA 449 F1 *Jupiter ®, Netzsch,* Germany) in DTA-TG configuration. The measurements were carried out under the flow of synthetic air and using the TG curves of as-received powder subjected to the similar suspesnion preparation without using the dispersant as the reference for weight loss.

A scanning electron microscope, SEM, (JEOL 7600F, JEOL, Tokyo, Japan) equipped with an energy dispersive X-ray spectrometer (EDXS, Oxford Instruments, UK) was used to examine the samples' microstructure on the fracture surface of the sintered bodies. Small samples were cut from the centre of the sintered bodies, ground and polished using 0.5 μm sized diamond slurries. The samples were cleaned in an ultrasonic bath with acetone. Afterwards, the samples were subjected to thermal etching at 1450 °C for 5 min in an electric furnace.

3. Results

The particle size distribution in suspensions, comprised of 5 vol% of solid fraction of $MgAl_2O_4$ and 5 wt% of the dispersant, after milling for 8, 24 and 72 h is shown in Fig. 1. The particle size distribution of as-received powder is also shown for comparison. The as-received powder contains two populations of agglomerates with a diameter of 2.5 μm and 0.55 μm. By assuming particles as spheres, one can calculate the size of elementary particles, d, using:

$$d = \frac{6}{SSA \times \rho} \quad (1)$$

where SSA is the specific surface area of the powder (26 $m^2 g^{-1}$) and ρ being the density (3.58 g cm^{-3}). The measured particle size is significantly larger than the estimated particle size (550 nm vs 64 nm), indicating that the as-received powder is highly agglomerated. Ball-milling for 8 h breaks the large bundles producing smaller agglomerates with an average diameter of 550 nm. Further ball-milling (24 h) produces a suspension characterised by two groups of particles: a minute portion with an average size of 70 nm representing powder's primary particles, and a large population consisting of agglomerates with a size between 180 and 300 nm. Further extension of milling time to 72 h causes re-agglomeration, producing large bundles several microns in diameter.

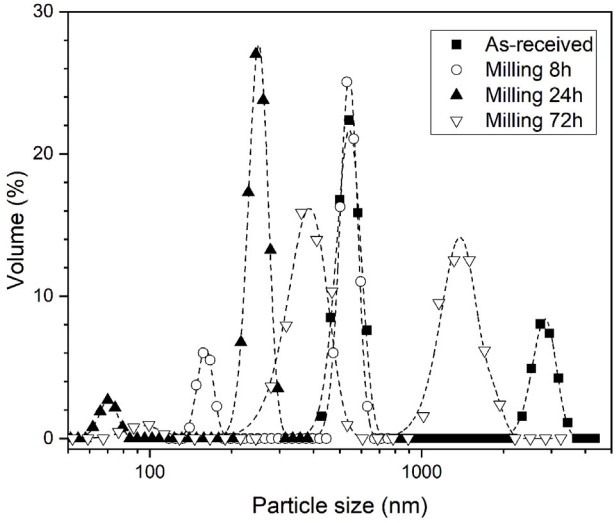

Fig. 1. Particle size distribution of $MgAl_2O_4$ powders after ball milling for 8,24 and 72 h. The data is acquired using dynamic light scattering. The particle size distribution of the as-received power is also shown for comparison.

Fig. 2 presents a part of the EDX spectra collected from solid particles after drying the suspension. Each spectrum was collected over a rectangular area (20 × 20 μm^2). The spectrum collected from a sintered body is also presented. In addition to magnesium, also aluminium as the second main component of spinel, and zirconium were detected, the latter in particular in the suspensions subjected to ball-milling for 72 h. The extensive milling is thus responsible not only for powder re-agglomeration but also results in marked contamination of the powder through the wear of milling balls. Preparation of highly dense spinel ceramic is the main goal of the present work: the influence of zirconia contamination on the rheological behaviour of the suspension was therefore not studied in detail.

No calcium was detected in samples using EDXS spectroscopy. Although calcium can be introduced to the samples through the dissolution of gypsum mould, its concentration was significantly below the

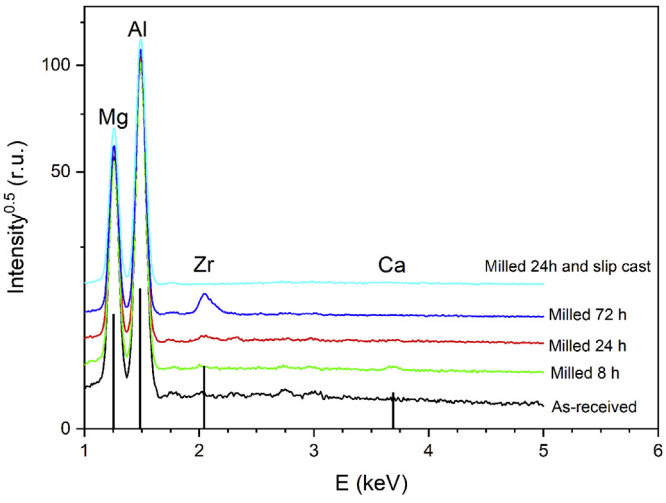

Fig. 2. EDXS spectra recorded on powders subjected to ball milling for different times of ball-milling using YTZ milling media; the recorded spectrum on the samples fabricated from a suspension after 24 h of milling, after sintering at 1550 °C for 2 h is also shown.

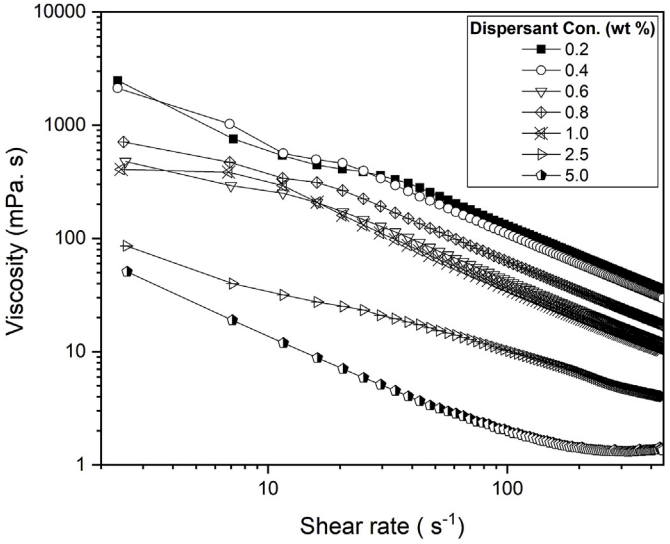

Fig. 3. Viscosity as a function of shear rate for suspensions containing various amount of dispersant. The suspension were prepared using 5 vol% spinel powder and ball milling for 24 h.

detection limit of the used characterisation method [29].

Fig. 3 shows the viscosity against the shear rate for suspensions with various dispersant active parts ranging between 0.2 and 5 wt% of the dispersant. The solid fraction was kept constant at 5 vol%. All suspensions exhibit shear thinning behaviour. However, the suspension containing 5 wt% of dispersant shows Newtonian behaviour at shear rates larger than 200 s^{-1}.

Fig. 4 summarises the results of viscosity measurements against the solid fraction of suspensions with the dispersant concentration of 5 wt% at 200, 300 and 400 s^{-1}. The viscosity of suspensions increases with increasing solid loading. The experimental results were normalised with respect to the viscosity of water at the temperature of measurement, and the relative viscosity, η_r, was calculated. The data were further fitted with the use of the Krieger-Dougherty equation [30]:

$$\eta_r = \left(1 - \frac{\phi}{\phi_m}\right)^{-n} \quad (2)$$

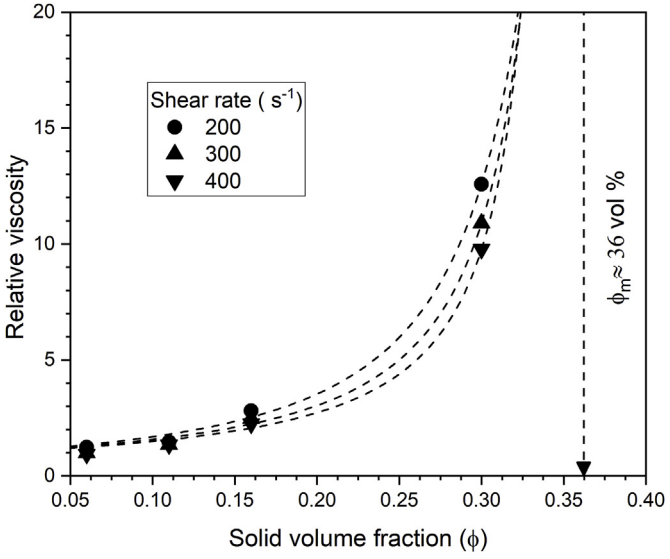

Fig. 4. Viscosity against the solid loading of $MgAl_2O_4$ suspensions containing 5 wt% of the dispersant after ball milling for 24 h. The viscosity was measured at 200, 300 and 400 s^{-1}.

Table 1
Krieger-Dougherty equation parameters estimated from fitting the experimental results (shown in Fig. 4) to Eq. (2). The numbers between parentheses are standard error of calculation.

Dispersant Concentration (wt %)		Shear rate (s^{-1})		
		200	300	400
5	ϕ_m	0.40 (0.02)	0.37 (0.02)	0.35 (0.03)
	n	1.81 (0.23)	1.42 (0.20)	1.20 (0.32)

where ϕ is the volume fraction of solid particles in the suspension. ϕ_m and n are the fitting parameters: ϕ_m is attributed to the solid fraction at which the suspension behaviour is similar to that of a solid body (infinite viscosity), and n describes the relation between the viscosity and the concentration of solid particles. The fitting parameters are summarised in Table 1.

The maximum solid loading for the suspensions containing the dispersant concentration of 5 wt% is $\phi_m = 0.37$, which is about the 68 wt% of solid loading and is significantly larger than the reported solid loading in literature [24,25]. Moreover, n is almost independent of the applied shear rate; this implies that the particles can move freely in suspensions containing 5 wt% of the dispersant [31]. It is worth investigating the viscosity of suspensions containing large amounts of solid loading; Fig. 5 shows the viscosity as a function of shear rate for suspensions comprising 2.5–8 wt% of dispersant, and solid loading of 15 and 30 vol%. The mixtures containing a dispersant concentration smaller than 2.5 wt% and solid loading of 15 vol% were paste-like and unsuitable for slip casting. Although the viscosity decreases continuously with the dispersant concentration increase, the variation of viscosity is limited at the dispersant concentrations larger than 3.3 wt%. The suspensions viscosity was significantly increased when larger amounts of solid loading (30 vol%) is used; the suspensions containing less than 3.3 wt% of dispersant exhibit a paste-like behaviour. Interestingly, the mixtures containing a dispersant concentration of 6 and 8 wt% also behave as a paste; such behaviour implies that the excessive amounts of dispersant might produce a structure in suspension that prevents the particles movement; this makes de-airing and casting of suspensions impossible. Among the suspensions comprising 30 vol% of solid loading, the suspension containing 5 wt% of dispersant shows the lowest viscosity. Such an amount is comparable with the dispersant concentration for producing suspensions from similar magnesium aluminate spinel powder: 4 wt% of Ammonium polyacrylic acid and 20 vol % solid loading reported by Kim et al. [24], or 5 wt% of Ammonium polyacrylate and pH modification of suspensions containing 30 vol% of solid loading reported by Kadosh et al. [19].

The green bodies produced by slip casting were dried at 50 °C for 48 h and, afterwards, the weight loss associated with the burn-out of the dispersant was measured by performing DTA/TG and using the as-received powder as reference. Fig. 6 shows the result of DTA/TG analysis of samples, produced from suspensions containing 5 wt% dispersant. The broad exothermic peak between 150 and 550 °C is mainly corresponding to the burn-out of the dispersant present in the green bodies; however, the weight loss is significantly smaller than the added dispersant to the powder (1.6 wt% vs 5 wt%). There is a certain amount of dispersant that remains in samples, and the excess dispersant is removed during the casting process [32]. Although the remaining dispersant can be removed by burn-out at 450 °C, it should be noted that higher addition of the dispersant makes its removal unnecessarily complicated with no beneficial influence on the suspensions' viscosity.

Table 2 summarises the relative density and open porosity of samples fabricated from suspensions with various solid loading sintered at 1550 °C for 2 h. The density slightly increases with increasing solid loading of suspension; the open porosity of samples produced from

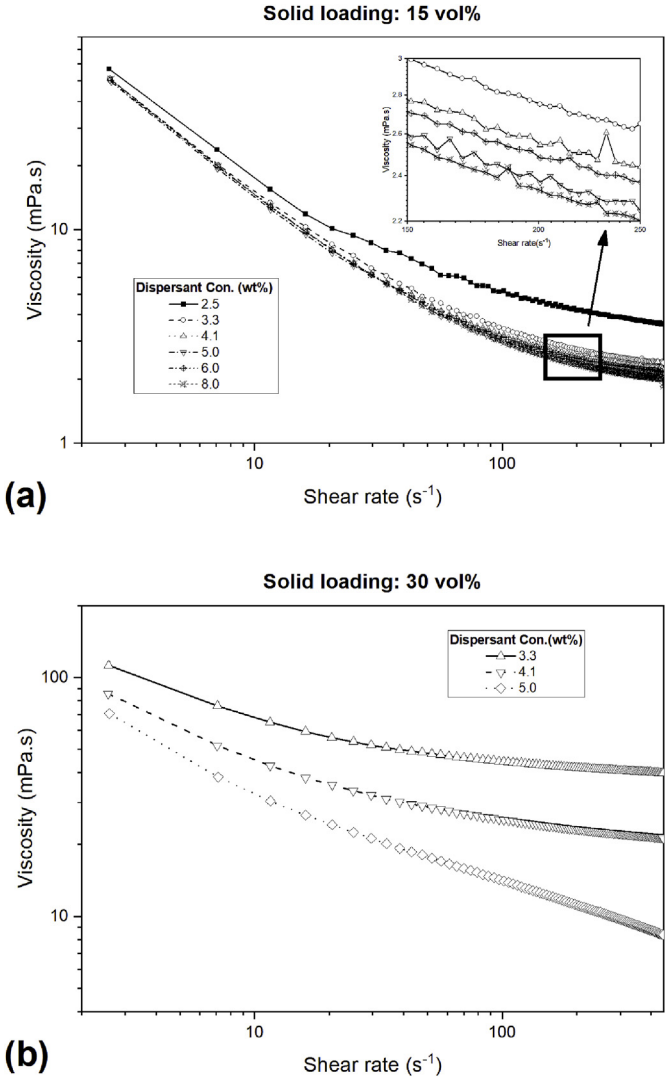

Fig. 5. Viscosity againts shear rate for suspensions containing various amount of dispersant (dispersant concentration wt%). The suspensions were prepared using (a) 15 vol% and (b) 30 vol% spinel powder.

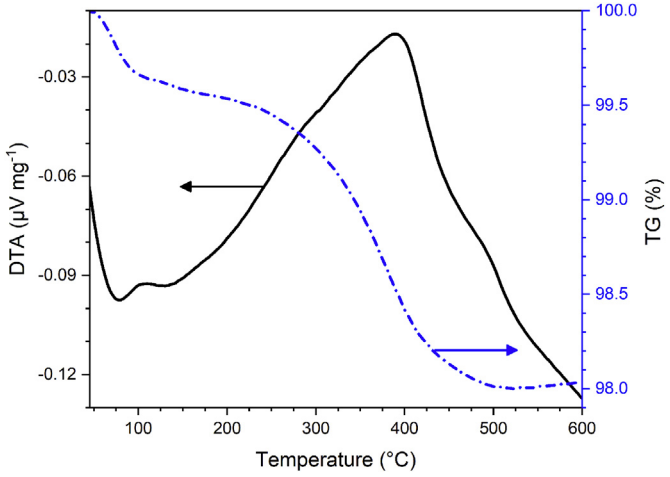

Fig. 6. DTA/TG curves for samples produced using 30 vol% suspensions and containing 5 wt% of Dolapix CE64; the as-received powder was used as reference.

Table 2
Relative density and open porosity of samples sintered at 1550 °C for 2 h; samples were fabricated using suspension containing 5 wt% of dispersant and different solid fraction. The standard deviation is shown between parentheses.

Solid fraction (vol%)	Relative density (%)	Open porosity (%)
10	97.51 (0.08)	0.12 (0.02)
15	97.56 (0.04)	0.03 (0.01)
30	98.08 (0.01)	0.00 (0.00)

30 vol% suspensions is almost completely removed during sintering.

Air bubbles can be trapped in samples during the consolidation process, particularly when a viscous suspension is used; the trapped air remains present in the form of large pores that cannot be eliminated by pressureless sintering.

It is worth noting that the shrinkage during sintering is clearly related to the solid fraction; using a higher solid loading decreases dimensional changes of samples during the densification. The samples' shrinkage, ($\Delta l/l_0$), during sintering can be calculated using Equation (3):

$$\frac{\Delta l}{l_0}(\%) = \frac{1}{3}.\left(1 - \frac{\rho_i}{\rho_f}\right) \times 100 \quad (3)$$

where ρ_I and ρ_f represent green and final density, respectively. Considering the density of samples annealed at 900 °C for 2 h as ρ_i (38.6% and 50.3% for 15 and 30 vol%, respectively) and the density after sintering at 1550 °C for 2 h (97.3% and 98.1%), the shrinkage during sintering is calculated to be 20% and 16% for samples fabricated from 15 to 30 vol% solid loading suspensions, respectively. Lower shrinkage improves the dimensional accuracy of produced components and, in turn, reduces possible sintering stresses and flows. The samples produced from suspensions with a low solid loading were deformed during drying and sintering. A large amount of water is present in the low solid loading suspensions; therefore, the total shrinkage of slip cast bodies, both after drying and sintering, increases with decreasing the solid loading of suspensions [33]. Moreover, removing a large amount of water during slip casting and drying is responsible for a density gradient and non-uniform shrinkage [34].

Fig. 7 shows the appearance of samples produced with 5, 15 and 30 vol% of solid loading and sintered at 1550 °C for 2 h. The samples were ground to the thickness of 1 mm and mirror polished using 0.5 µm diamond abrasive paper. The 30 vol% sample was translucent indicating that it contains only negligible concentration of small pores acting as light scattering sites.

Samples produced from 30 vol% suspensions were subjected to a sintering regime with a constant heating rate of 10 °C.min^{-1} up to 1550 °C. After heating the samples were removed from the furnace and quickly cooled down to room temperature to freeze the microstructure. Table 3 summarises the relative density and open porosity of the samples sintered in the temperature range between 900 and 1550 °C with different times of isothermal dwelling. The grain size of selected samples was measured from SEM micrographs of mirror polished and thermally etched cross sections. The grain size was estimated with the use of the Linecut method under the assumption that all grains were equiaxial [35,36]. The relative density of 98% was achieved already after 10 min sintering at 1550 °C. Isothermal heating for 30 min at the same temperature eliminates the open porosity so that the samples can be subjected to hot isostatic pressing without further preparation. Sintering for long time results in samples containing large grains, i.e. the samples sintered at 1550 °C for 4 h contain grains with a diameter larger than 30 µm.

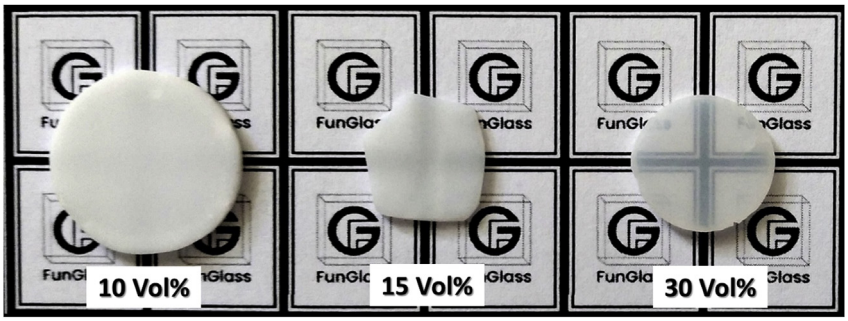

Fig. 7. Optical photographs of samples (1 mm in thickness) produced from suspensions with different concentrations of solid fraction. The samples were sintered at 1550 °C for 2 h; the samples are placed directly at the background.

Table 3
Relative density, open porosity and grain size of samples were fabricated using 30 vol % suspension. The samples sintered at different temperature and dwelling time. The standard deviation is shown between parentheses. (ND = not Determined).

Temperature (°C)	Dwelling time (min)	Relative density (%)	Open porosity (%)	Grain size (μm)
900	120	50.33 (0.34)	26.50 (0.85)	ND
1450	0	74.50 (0.02)	23.20 (0.01)	ND
1500	0	82.38 (0.04)	5.26 (0.02)	ND
1550	0	92.61 (0.20)	0.95 (0.01)	0.41 (0.15)
1550	10	97.92 (0.22)	0.06 (0.06)	0.56 (0.16)
1550	30	97.70 (0.29)	0.04 (0.03)	0.66 (0.24)
1550	60	98.08 (0.08)	0.00 (0.00)	0.82 (0.32)
1550	120	97.74 (0.08)	0.00 (0.01)	ND
1550	240	98.02 (0.00)	0.01 (0.01)	23.43 (8.31)

4. Discussion

4.1. Shaping

Ball-milling breaks soft agglomerates in ceramic powder producing smaller particles and the surface for the attachment of dispersant molecules. The SEM micrograph of dried suspension after 24 h of milling (Fig. 8), shows that it is composed of particles with an average diameter of 120 nm; however, the suspension is characterised by an average particle size between 180 and 300 nm using DLS method (Fig. 1). The results confirm that clusters of primary particles are still present in suspensions. Considering the narrow particle size distribution in suspensions, one can assume that the suspensions consist of symmetric clusters dispersed in liquid [37]. The ratio of the clusters' diameter determined by DLS technique to that measured by microscopy techniques (250 nm/120 nm ≈ 2) indicates that the clusters have a packed configuration of primary particles, almost entirely free of large pores acting as solid units to produce a homogeneous dense body [7,38].

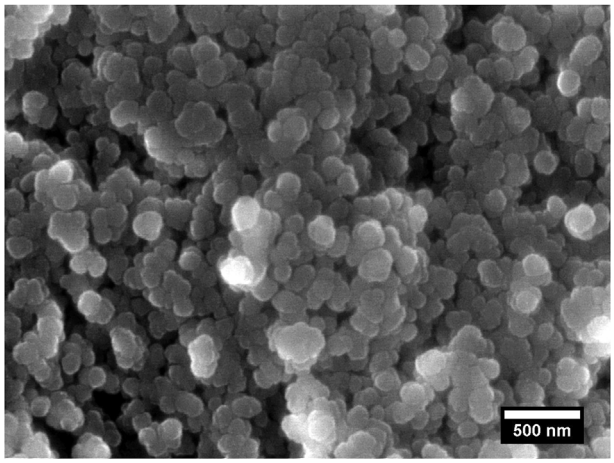

Fig. 8. SEM micrograph of the powder dried for 24 h at 105 °C after 24 h of ball-milling.

All suspensions exhibit shear thinning behaviour revealing that a structure of particles exists in suspensions that disintegrates by shear stress. Consequently, the viscosity continuously decreases upon applying shear stresses (Fig. 3) [20,31,39]. The viscosity is also strongly affected by the amount of added dispersant: it decreases rapidly at a concentration larger than 1 wt%. The suspensions with reasonable viscosity for slip casting were obtained when high concentrations of dispersant were used; this points out the role of the polyelectrolyte dispersant in increasing the inter-particle distance and, in turn, the long-range repulsion [20,40]. The small value of Einstein coefficient of suspensions containing 5 wt% of dispersant (n ≈ 1.6) indicates the free flow of particles in a reasonably dispersed suspension [41,42]. Suspensions with high solid loading but with low viscosity, suitable for slip casting, can be thus produced. Since no additives, such as NaOH or HNO_3, were used to modify the pH of suspensions and to produce electrostatic repulsion between the particles, the polymeric chains of the dispersant are responsible for the powder dispersion and stability of suspensions. The dispersant, Dolapix CE 64, is adsorbed at the particles surface through its functional groups (CH_3—C—CH_2—COO···NH_4). The polymeric chains are bound to the particles' surface through the interaction between COO^- groups and the Mg^{2+} and Al^{3+} cations of $MgAl_2O_4$ at the particles' surfaces [32]. The polyelectrolyte dispersant provides the repulsive forces between the particles and the powder is dispersed through the electrostatic mechanisms contributions.

Fig. 9 shows the fracture surface of the bodies fabricated from the suspension with 30 vol% solid loading and 5 wt% of dispersant annealed at 900 °C for 2 h. During slip-casting, the suspensions particles were aligned by the flow of liquid established through capillary forces implied by the porous mould: accumulation of particles at the surface of the mould produces the ceramic body [43]. Moreover, the interparticle distance of particles decreases when the dispersant is removed during slip casting, and the dispersed spherical particles produce a packed structure consisting of a continuous network of touching spheres. Moreover, such a packed structure of spheres is characterised by a packing fraction of about 54% which is in good agreement with the green density measured for bodies produced from suspensions with solid loading of 30 vol% [44,45].

The non-uniform distribution of density and large drying shrinkage of samples produced from the diluted suspensions are accounted for by the excessive water trapped between the particles during shaping. Although the packing of green bodies produced from suspensions containing 30 vol% of solid loading is not as high as the packed crystal structures, the interparticle porosity can be removed entirely by pressureless sintering. Moreover, due to the low viscosity, the suspension can be used for consolidation methods such as pressure casting and

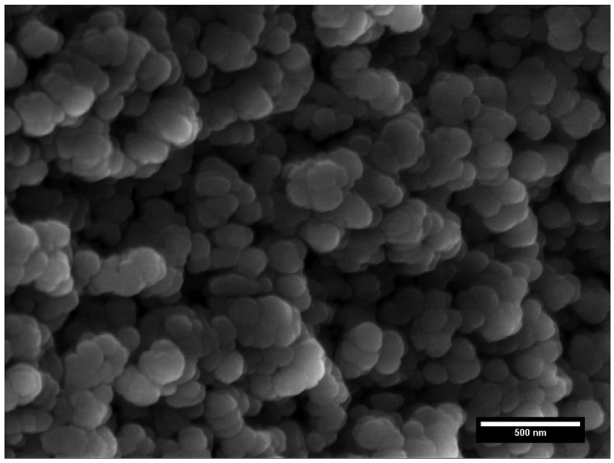

Fig. 9. Fracture surface of a green body prepared by casting of a suspension with 30 vol % solid loading and the AP = 1.15 mg m-2, heat-treated at 900 °C for 2 h.

vacuum filtration.

4.2. Sintering

Fig. 10 shows the fracture surfaces of samples prepared from the 30 vol% suspension sintered under different conditions. The spinel powder used in the present study (S30CR Baikowski) starts to densify around 1000 °C [18]. The particles are bonded together by the formation and growth of necks in the initial and the second stage of sintering at 1450 °C and 1500 °C. Treatments at a higher temperature (1550 °C) provides the required activation energy for densification. By dwelling at

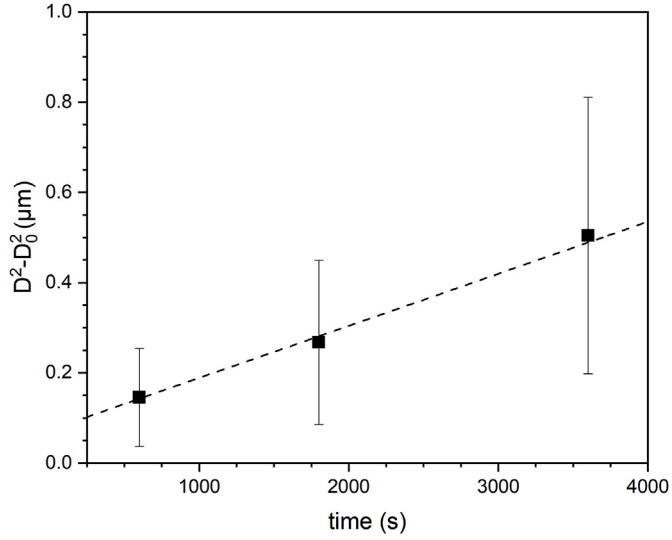

Fig. 11. Grain growth of $MgAl_2O_4$ samples produced by slip casting and sintered at 1550 °C; (R = 0.99).

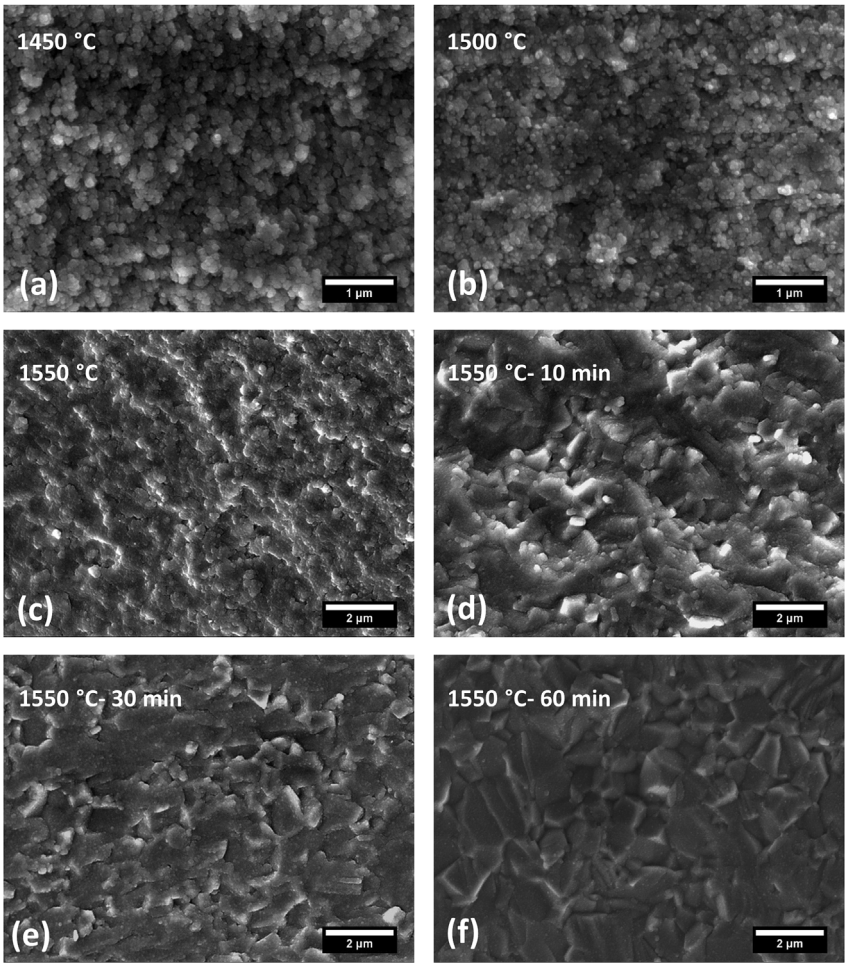

Fig. 10. Fracture surfaces of sintered spinel ceramics prepared from a suspension with 30 vol % solid loading after sintering without isothermal dwell at: (a) 1450 °C; (b) 1500 °C; (c) 1550 °C. The micrographs (d), (e) and (f) represent the fracture surfaces of samples isothermally heated at 1550 °C for 10, 30 and 60 min, respectively.

1550 °C, a uniform and dense body is produced after sintering for 30 min. Exposure to such a high temperature is, however, responsible for grain growth. It is also worth noting that prolonged isothermal heating causes coalescence of pores: the formed large pores then cannot be removed by further sintering or hot isostatic pressing. Consequently, sintering at 1550 °C for 10–30 min is likely to be the optimum condition for producing dense bodies using slip-casting/HIP approach.

Fig. 11 shows the dependence of grain size of samples sintered at 1550 °C as a function of dwell time. The measured grain size, Table 3, was fitted with the use of the grain growth law [46,47].

$$D^m - D_0^m = kt \quad (4)$$

where k is a constant depending on the mechanism controlling grain growth, D and D_0 being the grain size and initial grain size, respectively; t is time, and m is an exponent indicating the grain growth mechanism. The best fit is obtained when n = 2 is used, indicating diffusion being the only dominant mechanism of grain growth [46]. The influence of secondary phases on grain growth is proportional to the inclusions size and inversely proportional to their volume fraction in the matrix phase. The zirconium concentration is very limited according to the EDXS analyses (Fig. 2). Consequently, the volume fraction of zirconium oxide is lower than the minimum amount required to impede the grain growth by Zener pinning. However, any effect of zirconia impurities introduced from the milling media and segregated at grain boundaries without forming discrete second phase particles is not clear and will require further study.

Although no calcium was detected in the slip cast samples, minute amounts of calcium can be introduced through the dissolution of calcium sulfate in water from the gypsum mould during slip casting. Kim et al. have reported that calcium precipitated in the form of $CaO.2Al_2O_3$ at grain boundaries of $MgAl_2O_4$ at 1500 °C [25]. At higher temperatures $CaO.6Al_2O_3$ was identified as the secondary phase [48,49]. Calcium reacts with $MgAl_2O_4$ and produces liquid phases which can promote sintering. By increasing the temperature, the concentration of Al_2O_3 in the liquid phase increases by dissolution of spinel, and calcium aluminate phases precipitate out in the grain boundaries. However, based on the results obtained in this work, it is not clear whether the concentration of calcium contamination is sufficient for the formation of a liquid that influences the sintering process. Nevertheless, it should be noted that even small precipitates of calcium aluminate phases might have a significant scattering effect on final body transparency.

5. Conclusions

High solid loading suspensions of magnesium aluminate spinel with low viscosity suitable for slip casting were produced by exclusively using polyelectrolyte dispersing agent. The suspensions viscosity is affected by the dispersant concentration and solid loading: the dispersant addition larger than 5 wt% to the mixtures containing 30 vol% of solid loading produces paste-like suspensions, whereas suspension comprising 15 vol% of solid loading exhibit no increase in viscosity with the increase of dispersant concentration.

Green density of slip cast samples was affected by both the solid loading and the dispersant concentration in suspensions. Translucent spinel bodies were fabricated from suspensions with a 30 vol% solid loading: the ability to produce close packing configurations of particles is responsible for obtaining green bodies with porosity readily removable by pressureless sintering.

Acknowledgement

This paper is a part of dissemination activities of the project FunGlass. This project has received funding from the European Union´s Horizon 2020 research and innovation programme under grant agreement No 739566. Financial support of this work by the grants SAS-MOST JRP 2015/6, and VEGA 2/0026/17 is gratefully acknowledged. We appreciate the assistance of Dr. H. El-Maghraby for viscosity measurments.

References

[1] I. Ganesh, A review on magnesium aluminate (MgAl2O4) spinel: synthesis, processing and applications, Int. Mater. Rev. 58 (2013) 63–112.
[2] N.M. Khalil, M.B. Hassan, E.M.M. Ewais, F.A. Saleh, Sintering, mechanical and refractory properties of MA spinel prepared via co-precipitation and sol–gel techniques, J. Alloy. Comp. 496 (2010) 600-6007.
[3] I. Reimanis, H.J. Kleebe, A review on the sintering and microstructure development of transparent spinel (MgAl2O4), J. Am. Ceram. Soc. 92 (2009) 1472–1480.
[4] M. Rubat du Merac, H.-J. Kleebe, M.M. Müller, I.E. Reimanis, Fifty years of research and development coming to fruition; unraveling the complex interactions during processing of transparent magnesium aluminate (MgAl2O4) spinel, J. Am. Ceram. Soc. 96 (2013) 3341–3365.
[5] A. Rothman, S. Kalabukhov, N. Sverdlov, M.P. Dariel, N. Frage, The effect of grain size on the mechanical and optical properties of spark plasma sintering-processed magnesium aluminate spinel MgAl2O4, Int. J. Appl. Ceram. Technol. 11 (2014) 146–153.
[6] S.F. Wang, J. Zhang, D.W. Luo, F. Gu, D.Y. Tang, Z.L. Dong, G.E.B. Tan, W.X. Que, T.S. Zhang, S. Li, L.B. Kong, Transparent ceramics: processing, materials and applications, Prog. Solid State Chem. 41 (2013) 20–54.
[7] A. Goldstein, Correlation between MgAl2O4-spinel structure, processing factors and functional properties of transparent parts (progress review), J. Eur. Ceram. Soc. 32 (2012) 2869–2886.
[8] K.E. Sickafus, J.M. Wills, N.W. Grimes, Structure of spinel, J. Am. Ceram. Soc. 82 (2004) 3279–3292.
[9] L. Esposito, A. Piancastelli, S. Martelli, Production and characterization of transparent MgAl2O4 prepared by hot pressing, J. Eur. Ceram. Soc. 33 (2013) 737–747.
[10] K. Morita, B.-N. Kim, H. Yoshida, K. Hiraga, Densification behavior of a fine-grained MgAl2O4 spinel during spark plasma sintering (SPS), Scripta Mater. 63 (2010) 565–568.
[11] M. Sokol, M. Halabi, S. Kalabukhov, N. Frage, Nano-structured MgAl2O4 spinel consolidated by high pressure spark plasma sintering (HPSPS), J. Eur. Ceram. Soc. 37 (2017) 755–762.
[12] M. Sokol, S. Kalabukhov, M.P. Dariel, N. Frage, High-pressure spark plasma sintering (SPS) of transparent polycrystalline magnesium aluminate spinel (PMAS), J. Eur. Ceram. Soc. 34 (2014) 4305–4310.
[13] A. Krell, T. Hutzler, J. Klimke, A. Potthoff, Fine-Grained transparent spinel windows by the processing of different nanopowders, J. Am. Ceram. Soc. 93 (2010) 2656–2666.
[14] A. Krell, A. Bales, Grain size-dependent hardness of transparent magnesium aluminate spinel, Int. J. Appl. Ceram. Technol. 8 (2011) 1108–1114.
[15] C. Gajdowski, J. Bohmler, Y. Lorgouilloux, S. Lemonnier, S. d'Astorg, E. Barraud, A. Leriche, Influence of post-HIP temperature on microstructural and optical properties of pure MgAl2O4 spinel: from opaque to transparent ceramics, J. Eur. Ceram. Soc. 37 (2017) 5347–5351.
[16] Z. Jie, L. Tiecheng, C. Xianghui, W. Nian, X. Wen, Related mechanism of transparency in MgAl 2 O 4 nano-ceramics prepared by sintering under high pressure and low temperature, J. Phys. D Appl. Phys. 42 (2009) 052002.
[17] P. Ramavath, P. Biswas, K. Rajeswari, M.B. Suresh, R. Johnson, G. Padmanabham, C.S. Kumbhar, T.K. Chongdar, N.M. Gokhale, Optical and mechanical properties of compaction and slip cast processed transparent polycrystalline spinel ceramics, Ceram. Int. 40 (2014) 5575–5581.
[18] N. Benameur, G. Bernard-Granger, A. Addad, S. Raffy, C. Guizard, Sintering analysis of a fine-grained alumina-magnesia spinel powder, J. Am. Ceram. Soc. 94 (2011) 1388–1396.
[19] T. Kadosh, Y. Cohen, Y. Talmon, W.D. Kaplan, In situ characterization of spinel nanoceramic suspensions, J. Am. Ceram. Soc. 95 (2012) 3103–3108.
[20] J.A. Lewis, Colloidal processing of ceramics, J. Am. Ceram. Soc. 83 (2004) 2341–2359.
[21] P.P. Zhang, P. Liu, Y. Sun, J. Wang, Z.J. Wang, S.W. Wang, J. Zhang, Aqueous gelcasting of the transparent MgAl2O4 spinel ceramics, J. Alloy. Comp. 646 (2015) 833–836.
[22] M. Krishnan, B. Tiwari, S. Seema, K.-N. of Materials, ... , Transparent magnesium aluminate spinel: a prospective biomaterial for esthetic orthodontic brackets, J. Mater. Sci. Mater. Med. 25 (2014) 2591–2599.
[23] A. Shafeiey, M.H. Enayati, A. Al-Haji, The effect of slip casting parameters on the green density of MgAl2O4 spinel, Ceram. Int. 43 (2017) 6069–6074.
[24] J.M. Kim, H.N. Kim, Y.J. Park, J.W. Ko, J.W. Lee, H.D. Kim, Fabrication of transparent MgAl2O4 spinel through homogenous green compaction by microfluidization and slip casting, Ceram. Int. 41 (2015) 13354–13360.
[25] J.-M. Kim, H.-N. Kim, Y.-J. Park, J.-W. Ko, J.-W. Lee, H.-D. Kim, Microstructure and optical properties of transparent MgAl 2 O 4 prepared by Ca-infiltrated slip-casting and sinter-HIP process, J. Eur. Ceram. Soc. 36 (2016) 2027–2034.
[26] I. Ganesh, Aqueous slip casting of MgAl2O4 spinel powder, Bull. Mater. Sci. 34 (2011) 327–335.
[27] I. Ganesh, G. Sundararajan, J.M.F. Ferreira, Aqueous slip casting and hydrolysis assisted solidification of MgAl2O4 spinel ceramics, Adv. Appl. Ceram. 110 (2011) 63–69.
[28] I. Ganesh, G.J. Reddy, G. Sundararajan, S.M. Olhero, P.M.C. Torres, J.M.F. Ferreira, Influence of processing route on microstructure and mechanical properties of MgAl2O4 spinel, Ceram. Int. 36 (2010) 473–482.

[29] J.I. Goldstein, D.E. Newbury, J.R. Michael, N.W.M. Ritchie, J.H.J. Scott, D.C. Joy, Scanning Electron Microscopy and X-Ray Microanalysis, Springer New York, 2017.
[30] W.J. Frith, A. Lips, The rheology of concentrated suspensions of deformable particles, Adv. Colloid Interface Sci. 61 (1995) 161–189.
[31] L. Bergstrom, Shear thinning and shear thickening of concentrated ceramic suspensions, Colloid. Surf. Physicochem. Eng. Asp. 133 (1998) 151–155.
[32] S. Mei, J. Yang, J.M.F. Ferreira, Effect of dispersant concentration on slip casting of cordierite-based glass ceramics, J. Colloid Interface Sci. 241 (2001) 417–421.
[33] G. Tarì, J.M.F. Ferreira, Influence of solid loading on drying-Shrinkage behaviour of slip cast bodies, J. Eur. Ceram. Soc. 18 (1998) 487–493.
[34] J.D. Yates, S.J. Lombardo, Effect of solids loading and dispersant concentration on strain mismatch and deformation of slip-cast green bodies, J. Am. Ceram. Soc. 84 (2001) 2274–2280.
[35] A. Thorvaldsen, The intercept method—2. Determination of spatial grain size, Acta Mater. 45 (1997) 595–600.
[36] A. Thorvaldsen, The intercept method—1. Evaluation of grain shape, Acta Mater. 45 (1997) 587–594.
[37] W.-P.J. chemistry, Measurement of special nanoparticle structures by light scattering, Anal. Chem. 86 (2014) 7171–7183.
[38] F.F. Lange, Sinterability of agglomerated powders, J. Am. Ceram. Soc. 67 (1984) 83–89.
[39] S. Gürgen, W. Li, M.C. Kuşhan, The rheology of shear thickening fluids with various ceramic particle additives, Mater. Des. 104 (2016) 312–319.
[40] J.S. Chong, E.B. Christiansen, A.D. Baer, Rheology of concentrated suspensions, J. Appl. Polym. Sci. 15 (1971) 2007–2021.
[41] K. Okada, Y. Nagase, Viscosity and powder dispersion in ceramic injection molding mixtures, J. Chem. Eng. Jpn. 33 (2000) 168–173.
[42] J.M.F. Ferreira, H.M.M. Diz, Effect of solids loading on slip-casting performance of silicon carbide slurries, J. Am. Ceram. Soc. 82 (1999) 1993–2000.
[43] F.M. Tiller, C.-D. Tsai, Theory of filtration of ceramics: I, slip casting, J. Am. Ceram. Soc. 69 (1986) 882–887.
[44] G.Y. Onoda, E.G. Liniger, Random loose packings of uniform spheres and the dilatancy onset, Phys. Rev. Lett. 64 (1990) 2727–2730.
[45] K.J. Dong, R.Y. Yang, R.P. Zou, A.B. Yu, Role of interparticle forces in the formation of random loose packing, Phys. Rev. Lett. 96 (2006) 145505.
[46] M.N. Rahaman, Sintering of Ceramics, CRC Press, 2007.
[47] R. Chaim, A. Shlayer, C. Estournes, Densification of nanocrystalline Y2O3 ceramic powder by spark plasma sintering, J. Eur. Ceram. Soc. 29 (2009) 91–98.
[48] D.A. Jerebtsov, G.G. Mikhailov, Phase diagram of CaO–Al2O3 system, Ceram. Int. 27 (2001) 25–28.
[49] Y.P. Tian, X.L. Pan, H.Y. Yu, G.F. Tu, Formation mechanism of calcium aluminate compounds based on high-temperature solid-state reaction, J. Alloy. Comp. 670 (2016) 96–104.